Contents lists available at ScienceDirect

Ultramicroscopy

Homogeneity and composition of AlInGaN: A multiprobe nanostructure study

Florian F. Krause [a,*], Jan-Philipp Ahl [b], Darius Tytko [c], Pyuck-Pa Choi [c], Ricardo Egoavil [d], Marco Schowalter [a], Thorsten Mehrtens [a], Knut Müller-Caspary [a], Johan Verbeeck [d], Dierk Raabe [c], Joachim Hertkorn [b], Karl Engl [b], Andreas Rosenauer [a]

[a] Institut für Festkörperphysik, Universität Bremen, Otto-Hahn-Allee 1, 28359 Bremen, Germany
[b] OSRAM Opto Semiconductors GmbH, Leibnizstr. 4, 93055 Regensburg, Germany
[c] Max-Planck-Institut für Eisenforschung GmbH, Max-Planck-Str. 1, 40237 Düsseldorf , Germany
[d] EMAT, Universiteit Antwerpen, Groenenborgerlaan 171, 2020 Antwerpen, Belgium

ARTICLE INFO

ABSTRACT

The electronic properties of quaternary AlInGaN devices significantly depend on the homogeneity of the alloy. The identification of compositional fluctuations or verification of random-alloy distribution is hence of grave importance. Here, a comprehensive multiprobe study of composition and compositional homogeneity is presented, investigating AlInGaN layers with indium concentrations ranging from 0 to 17 at% and aluminium concentrations between 0 and 39 at% employing high-angle annular dark field scanning electron microscopy (HAADF STEM), energy dispersive X-ray spectroscopy (EDX) and atom probe tomography (APT). EDX mappings reveal distributions of local concentrations which are in good agreement with random alloy atomic distributions. This was hence investigated with HAADF STEM by comparison with theoretical random alloy expectations using statistical tests. To validate the performance of these tests, HAADF STEM image simulations were carried out for the case of a random-alloy distribution of atoms and for the case of In-rich clusters with nanometer dimensions. The investigated samples, which were grown by metal-organic vapor phase epitaxy (MOVPE), were thereby found to be homogeneous on this nanometer scale. Analysis of reconstructions obtained from APT measurements yielded matching results. Though HAADF STEM only allows for the reduction of possible combinations of indium and aluminium concentrations to the proximity of isolines in the two-dimensional composition space. The observed ranges of composition are in good agreement with the EDX and APT results within the respective precisions.

© 2015 Elsevier B.V. All rights reserved.

1. Introduction

Quaternary AlInGaN has attracted increasing attention in the past years for the design of blue light emitting diodes (LEDs) [1,2] and field-effect transistors (FETs) [3,4]. The material benefits from its additional degree of freedom opposed to ternary systems, which to a certain extent allows an independent choice of either bandgap and lattice constant, allowing for the realisation of lattice-matched structures, or bandgap and polarisation, enabling the so-called polarisation-matched growth of AlInGaN/GaN hetero-structures. In these structures, polarisation effects such as the quantum-confined Stark effect are reduced, which is expected to lead to an increase in efficiency [5].

Besides the matching of polarisation, homogeneity of the alloy as well as defect density and morphology of the interfaces governs the electronic properties of AlInGaN-based devices [6–9]. Spectral width and efficiency of the emission of light from quantum wells (QWs) strongly depend on the distribution of indium, aluminium and gallium atoms within the wells. Some publications reported observations of indium-rich cluster formation, catalysed by the presence of aluminium in the quaternary material opposed to ternary InGaN [10,11]. Matsuoka [12] even found an unstable mixing region covering most of the quaternary composition space, whereas Marques et al. [13] predicted a phase transition from clustering to homogeneous mixing behaviour at ≈800 °C growth temperature. The present work demonstrates a comprehensive investigation of compositional homogeneity in AlInGaN layers grown by metal-organic vapour phase epitaxy (MOVPE) employing different high-resolution experimental methods, specifically, energy dispersive X-ray spectroscopy (EDX), high-angle annular

dark field scanning transmission electron microscopy (HAADF STEM) and atom-probe tomography (APT).

HAADF STEM has already been successfully used for the investigation of composition and compositional homogeneity in ternary materials such as AlGaN, InGaN or InAlN [14–16]. It benefits from the reduced beam damage compared to parallel illumination [17,15]. For the quaternary material $Al_x In_y Ga_{1-x-y}N$, however, measurement of indium and aluminium concentrations would require two separate inequivalent measured quantities. Thus, HAADF STEM measurements alone do not allow for determination of the composition in AlInGaN.

EDX, however, which is available during STEM measurements in modern electron microscopes, makes the simultaneous determination of both concentrations possible. With high brightness electron sources, probe correctors and windowless four-quadrant X-ray detectors it can even reach atomic resolution today [18]. For the investigation of possible clustering on the nanometer scale, however, long acquisition times are necessary to reach sufficient statistical significance, during which specimen drift can occur, cumbering the statistical analysis. Furthermore, as the resulting composition map is a two-dimensional projection of the specimen, in general corresponding simulations would be necessary to understand the exact volume of interaction in dependence of probe position.

APT-investigations overcome both disadvantages, as in these reconstructions both the type and the initial position of each detected ion are determined, allowing for a three-dimensional investigation of the spatial distribution of all species with respect to all other species. The crystal volume which is accessible in one measurement is, however, limited even compared to the nanometer-thin TEM-lamellas due to the sharp needle shape of the APT specimen.

In the following, a comprehensive study of composition and homogeneity of AlInGaN with various concentrations using all methods mentioned above is presented. Samples with nominal compositions as listed in Table 1, comprising layers with four different aluminium concentrations between 0 and 39 at% and 12 at% In as well as AlGaN layers with nominal 39 at% Al, were investigated.

2. Specimens and instrumentation

The specimen primarily investigated here consists of 5 consecutive layers of AlInGaN of different concentrations embedded in GaN. It was grown by MOVPE on GaN/sapphire templates. Each layer is ≈10 nm thick and is separated from the next layer by a barrier of ≈50 nm GaN. They were grown far from thermodynamic equilibrium [19] at a temperature of 760 °C and a pressure of 200 hPa. A more detailed description of the growth and investigation of the surface morphology is given in the publication of Ahl et al. [20]. Two of the layers consist of InGaN and AlGaN,

Table 1
Nominal aluminium and indium concentrations of the five investigated compositions and the values measured by the different methods. The given errors were estimated from consecutive measurements of the same sample.

Composition	Nom. (at%)		XPS (at%) [20]		EDX (at%)		APT (at%)	
	Al	In	Al	In	Al	In	Al	In
no. 1	0	12	0 ± 0	13 ± 1	0 ± 0	10 ± 4	0 ± 0	12 ± 2
no. 2	13	12	13 ± 1	18 ± 1	17 ± 3	14 ± 3	16 ± 2	16 ± 2
no. 3	22	12	22 ± 1	20 ± 1	23 ± 3	16 ± 3	25 ± 2	16 ± 2
no. 4	39	12	39 ± 1	19 ± 1	33 ± 3	14 ± 3	31 ± 2	17 ± 2
no. 5	39	0	–	–	39 ± 3	0 ± 0	36 ± 2	0 ± 0
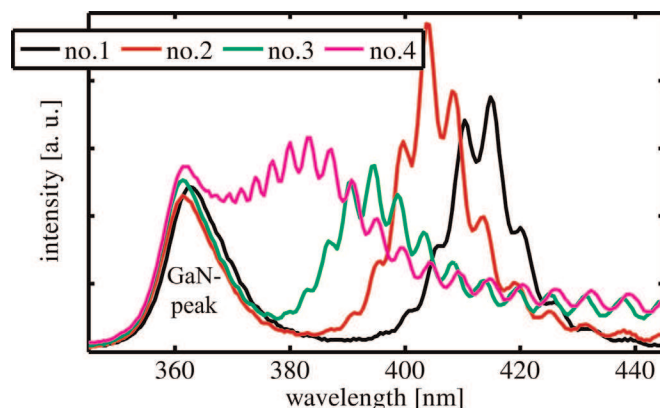
Fig. 1. PL-spectra of composition nos. 1–4: besides a blue-shift of the quaternary peak with rising aluminium content an increase of the peak-width can be observed. While the ternary material no. 1 exhibits a full width at a half maximum of 10 nm this increases to ≈27 nm for the composition with the highest aluminium content. The oscillations for wavelengths above the GaN peak are caused by Fabry–Perot interference in the GaN substrate.

respectively, providing ternary references for the investigations. Single-layer specimens with thicker layers but with the same nominal compositions were grown under identical conditions. These samples were used for the EDX measurements as they provide larger areas for simultaneous data acquisition within rectangular shaped areas of interest.

The first four compositions in Table 1 were pre-characterised by X-ray photoelectron spectroscopy (XPS) and photoluminescence spectroscopy (PL) [20]. The concentrations determined by XPS are also given in Table 1, whereas the spectra gained from the PL-measurement are depicted in Fig. 1. Besides the expected blue-shift for increasing aluminium concentrations, a broadening of the quaternary luminescence peak is observed. In the present paper, it is investigated, whether this increasing width is solely caused by the local concentration fluctuations inevitably occurring in a random alloy, which increase with the number of different constituents, or whether in addition indium clustering contributes to this effect.

A very thin sample was conventionally prepared by mechanical grinding and subsequent ion polishing for HAADF STEM, whereas for the EDX analyses, lamellas were prepared with a focused ion beam (FIB) using the lift-out method [21]. The samples were afterwards milled with low-energy Ar ions at 400 eV to remove etching damage [22]. The needle-shaped tip specimens for APT measurements were likewise prepared with a FIB using the lift-out method described in Ref. [23] and sharpened while successively reducing the ion energy from 30 kV to 2 kV.

EDX-maps were recorded with the XAntEM microscope of the University of Antwerp, a cubed FEI Titan[3] 60/300 G2 TEM with ChemiSTEM-design equipped with a high-brightness X-FEG, a probe aberration corrector and a windowless Super-X EDX-detector, which was operated at 300 kV. The HAADF STEM investigations were performed at a FEI Titan 80/300 G1 microscope also operated at 300 kV and equipped with a Fischione Model 3000 HAADF detector spanning from 30 to approximately 250 mrad. Atom probe tomography was conducted using a Cameca LEAP 3000X HR instrument.

3. Results and discussion

3.1. EDX-Investigation

First, the single-layer specimens with layers of the nominal compositions given in Table 1 and a thickness of (20 ± 5) nm were
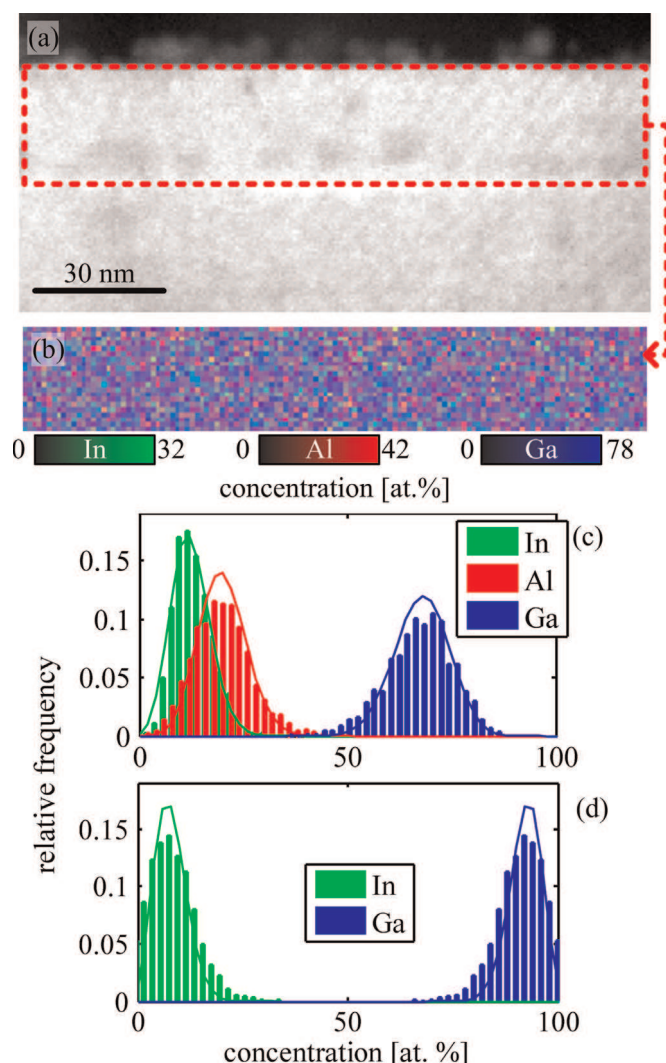
Fig. 2. Results of the EDX-investigation: (a) shows an HAADF STEM micrograph of the investigated area with the quaternary layer of composition no. 4 marked. The intensity fluctuations are caused by contamination during the long acquisition time of 10 min. The concentration map is displayed colour-coded in (b). From this, the histograms of indium, aluminium and gallium concentrations presented in (c) were determined. (d) shows the histograms for the ternary InGaN sample (composition no. 1) for comparison. The solid curves show the distributions expected for a homogeneous alloy. (For interpretation of the references to colour in this figure caption, the reader is referred to the web version of this paper.)

investigated by EDX. All samples were prepared as lamellas with a thickness of (40 ± 10) nm. EDX maps were acquired by drift-corrected, repetitive scanning of an area as shown in Fig. 2a for the quaternary specimen with the highest nominal aluminium concentration (no. 4 in Table 1), for which inhomogeneities are most likely to occur [12,13]. The scan time was chosen 10 min per spectrum-image with a pixel width of 6 Å to obtain a sufficiently high detection count rate for accurate quantification. For this the Cliff–Lorimer method [24] implemented in the proprietary Bruker ESPRIT software was used to evaluate the K-Lines of aluminium and gallium and the indium L-line with calculated k-factors of 1.00, 2.11 and 3.05, respectively, while the background subtraction was done with a polynomial fit from chosen background windows.

The resulting mean concentrations from averaging over the entire layer area are presented in Table 1, showing a generally good agreement with the nominal values. Fig. 2b displays the resulting composition map for the aluminium-rich sample with composition no. 4, which reveals an apparently homogeneous distribution of In, Al and Ga. To investigate the distributions

quantitatively, histograms of the relative frequencies of local In, Al and Ga concentrations were generated from the composition maps. They are shown in Fig. 2c for the map in Fig. 2b and for the ternary InGaN layer (composition no.1) in Fig. 2d for comparison. Using the mean concentration values determined by EDX in Table 1 as probabilities to detect In, Al and Ga atoms, a theoretical distribution of concentrations was calculated by 100 independent random draws per pixel, each of which results in the detection of either indium, aluminium or gallium. The number of draws was chosen to match the ternary sample best. It roughly corresponds to the number of atoms stacked in an atomic column at this specimen thickness. The binomial distributions, which represent ideal homogeneity due to the mutual independence of the draws, are shown in Fig. 2c and d as solid curves. Both samples show good agreement between measured and binomial distributions, no increased deviation is observed for the quaternary specimen. Admittedly the assumption of a binomial distribution and especially the reasoned but still somewhat arbitrary choice of 100 draws complicates the quantification of homogeneity from these data. For a less empirical model better knowledge of the interaction volume of the electron beam within the specimen of the X-ray propagation through the specimen and of the influence of detection and spectrum-quantification procedures would be required. However, the good representation of the experiment by the binomial model and the agreement being equally good for both the ternary and the quaternary sample are clear indications for a homogeneous alloy, though the meaningfulness is limited due to the mentioned lack of knowledge. Analogous evaluations were executed for both other quaternary concentrations in Table 1 yielding similar results.

3.2. HAADF STEM study

To further investigate the homogeneity of the AlInGaN alloys by statistical means, HAADF STEM images of AlInGaN crystals were simulated for various thicknesses with 31 at% Al and 16 at% In, corresponding to composition no. 4 in Table 1, where the metal atoms were set according to a completely random distribution. The simulations were conducted using the STEMsim software package [25] with the frozen-lattice multislice method [26,27]. Static atomic displacements (SADs) caused by the different covalent radii of the metal atoms were incorporated by force relaxation with the LAMMPS program package [28] employing the empirical Stillinger–Weber type potential proposed by Schowalter et al. [29] for Al–N and Ga–N bonds, while for In–N interactions parametrisation from Ref. [30] was used. The nonuniform sensitivity of the HAADF detector used in the following experiment was also taken into account [15]. The resulting images, a section of which is displayed in Fig. 3a, were evaluated atomic-column wise by averaging over Voronoi cells as described in Ref. [16]. To avoid discrepancies between experimental and simulated intensity distributions caused by slightly different mean concentrations, the intensities were divided by their mean, thereby centering the histograms around 1, as shown in Fig. 3b. This is justified, as the overall spread of intensities is less affected by small concentration changes than the mean intensity.

The resulting intensity ratio distribution is visually in very good agreement with a Gaussian distribution as can be seen in Fig. 3b. This agreement was also statistically tested: a chi-square goodness-of-fit test, which allows testing the hypothesis that the simulated values come from a Gaussian distribution by comparing the relative frequencies of simulation and ideal Gaussian distribution, confirms this hypothesis with a significance of 10% at all thicknesses. The one-sample Kolmogorov–Smirnov–Lilliefors test [31], which is a modification of the well-known Kolmogorov–Smirnov test taking into account that mean and standard
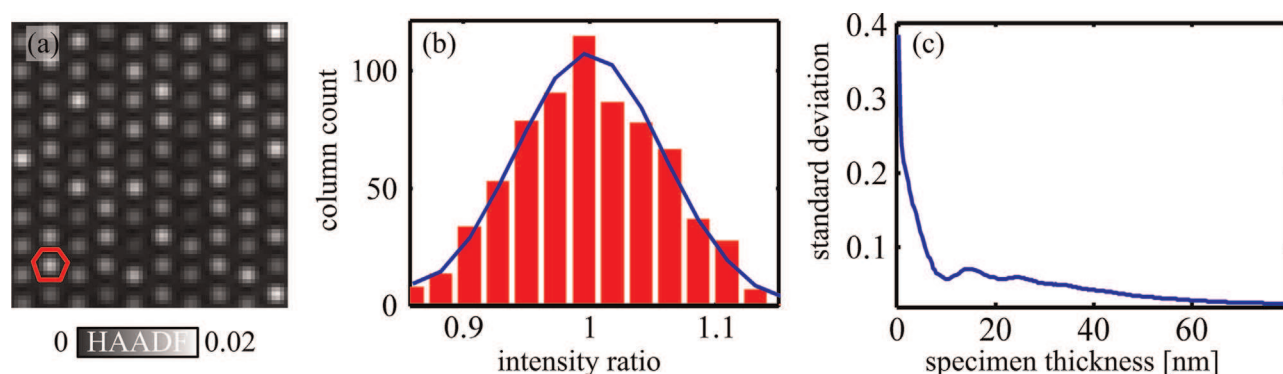
Fig. 3. HAADF STEM simulation of a random-alloy AlInGaN crystal with 31 at% Al and 16 at% In: in (a), a section of the image simulated for a specimen thickness of 2 nm is depicted. The red polygon exemplifies a Voronoi cell. Intensities averaged in Voronoi cells yield the histogram displayed in (b). The solid blue curve is the fitted Gaussian distribution. (c) depicts the standard deviation of the intensity ratio plotted vs. specimen thickness. (For interpretation of the references to colour in this figure caption, the reader is referred to the web version of this paper.)

deviation of the Gaussian distribution are not known in advance here, accepts even with 20% significance.

It shall be stressed here that the statistical significance represents the probability of erroneously rejecting the tested hypothesis, in this case that the underlying distribution is Gaussian. High significance does not necessarily imply that the probability to only accept the hypothesis if it is true, which is called the statistical power of the test, is also high, though it is commonly used to asses the results of a test. The test power has therefore also be checked which is done later in this section.

The standard deviation of the simulated intensity ratio is plotted in Fig. 3c. For very thin crystals with thicknesses below 10 nm it is varying rapidly with thickness, but for thicker specimens the variation of the standard deviation is smaller. A local maximum can be found at ≈15 nm. The following measurements were hence executed at this thickness to avoid an artificial increase of the obtained standard deviations by an error of the measured specimen thickness.

High-resolution HAADF STEM images were acquired accordingly at a specimen thickness of 16 ± 2 nm, which was measured from the intensity in the GaN areas. The intensity was normalised to the incident intensity [14–16] and evaluated in the same way as the simulated data before. An exemplary micrograph is shown in Fig. 4a.

In the experiment, the intensity of atom columns varies even in pure GaN. This noise is primarily caused by small thickness variations and surface contamination. In the following, it was assumed that the noise caused by these effects is the same in the quaternary layers.

However, it might be even larger in the AlInGaN as selective etching causing stronger thickness variations is more probable

there. Therefore, the noise with a standard deviation of 0.03 estimated from a GaN area as the one marked red in Fig. 4b can be considered as a lower bound for AlInGaN.

As standard deviations are added Pythagorean, the relative contribution of this noise to the standard deviation of 0.08 measured in the quaternary material is less than 8%. The suchlike characterised noise was added to the simulated data by adding Gaussian distributed random numbers with the according standard deviation. The resulting histogram is shown in Fig. 4c in red. With the noise added, the simulated data should be fully comparable to the experiment. Hence, the intensity ratio distribution was also determined from the measured intensity of the AlInGaN layer with composition no. 4 as marked in green in Fig. 4b, leading to the green histogram in Fig. 4c. Apparently, both distributions are similar. This could also be confirmed by various statistical tests: not only is the one-sample Kolmogorov–Smirnov–Lilliefors test accepting normality of the experimental distribution with 20% significance, as it did for the simulation.

The two-sample Kolmogorov–Smirnov test, which checks whether two samples are from the same not necessarily Gaussian distribution, also confirms that the STEM intensity in the quaternary material has the same distribution as the noise-incorporated simulation with an exceptional significance of 45%. In a further statistical examination, the identity of the variances of simulation and experiment was also accepted by a two-sample F-Test and Bartlett's test, which allow testing this identity, with 30% significance. The unity of this test results strongly indicates the identity of the measured HAADF-intensity and the one expected for an entirely random alloy and hence a homogeneous composition in the quaternary material.

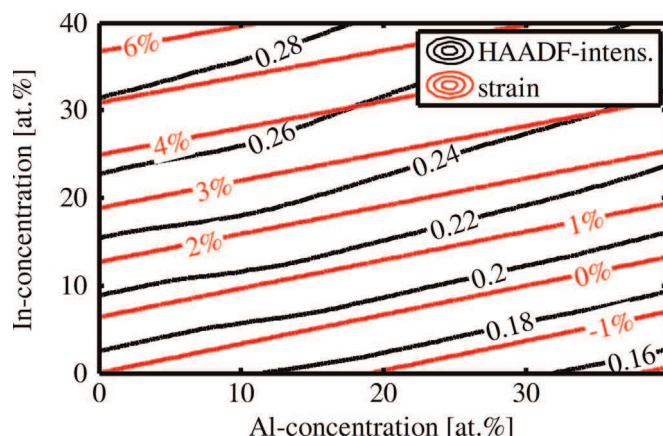However, as mentioned before, despite the very high
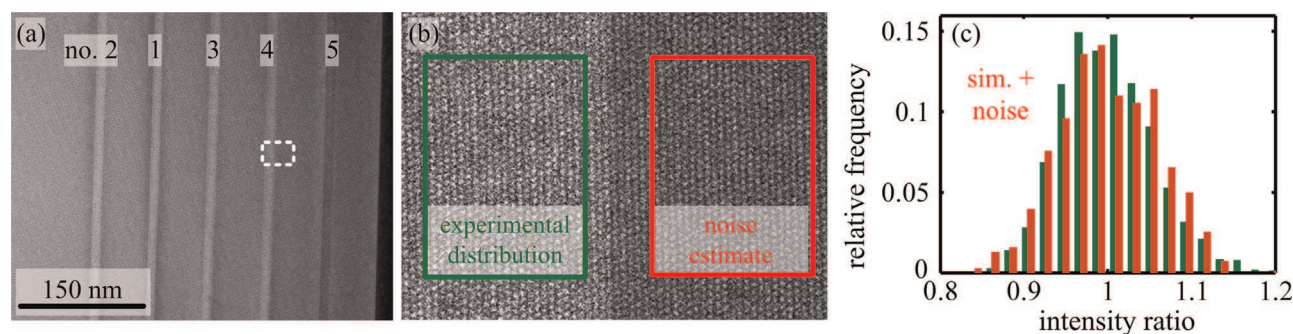
Fig. 4. Evaluation of the experimental HAADF STEM images: (a) is an overview of the investigated conventionally prepared specimen. The dotted rectangle marks the area, in which the high-resolution micrograph in (b) was taken. Averaging the image intensity over Voronoi cells yields an experimental noise estimate. (c) shows the experimental histogram from the analysis of the quaternary area marked by the green frame in (b) in direct comparison to the simulation results with incorporated noise marked by the red frame. (For interpretation of the references to colour in this figure caption, the reader is referred to the web version of this paper.)
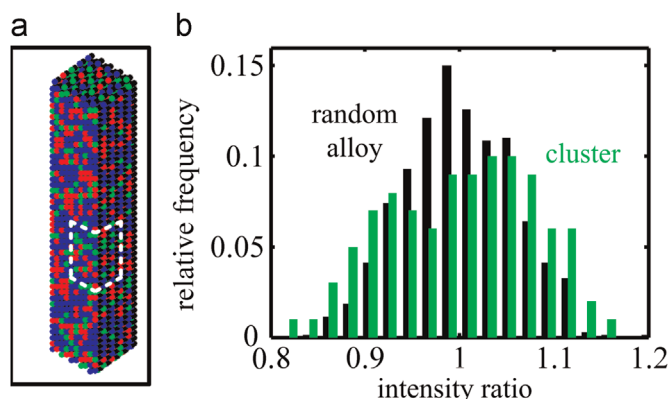
Fig. 5. Simulated HAADF STEM imaging of an indium-rich cluster: the supercell shown in (a) contains an indium-rich cluster marked by the dotted frame. The cubic-shaped cluster has a side length of 3 nm, the supercell is 15 nm high. The resulting histogram is shown in green in (b) in comparison to the distribution of a random alloy in black. (For interpretation of the references to colour in this figure caption, the reader is referred to the web version of this paper.)

Fig. 6. Comparison of HAADF STEM and strain reference data: The isolines of STEM intensity (normalised to the incident probe intensity) simulated with the frozen-lattice method and a specimen thickness of 50 nm are drawn in black, while the isolines of biaxial strain calculated by elasticity theory are plotted in red versus indium and aluminium concentrations. The red and black isolines run almost in parallel. (For interpretation of the references to colour in this figure caption, the reader is referred to the web version of this paper.)

significance with which the identity of distributions was accepted, the statistical power of the tests could still be small, if cluster-formation did not strongly alter the intensity-ratio distribution. To check against an error of this kind, another STEM simulation with a single cubic cluster with a side length of 3 nm with increased indium concentration of 40 at% and reduced aluminium concentration of 20 at% buried inside a supercell of 15 nm thickness was conducted. Size and composition of this cluster lies well in the range of inhomogeneities reported for AlInGaN [11,13]. The resulting image was evaluated as described above. The result is shown in Fig. 5 in direct comparison to the random-alloy distribution. These histograms are clearly different and in fact the two-sample Kolmogorov–Smirnov test rejects their identity and the one-sample Kolmogorov–Smirnov–Lilliefors test does not accept Gaussian distribution of the intensity ratio obtained for the simulated cluster, not even for a significance of only 1%. It can thus be concluded that the statistical analysis of HAADF STEM data presented here powerful enough and hence well-suited to exclude existence of nanometer-scale clusters with an indium concentration increased from approximately 20 at% to 40 at%. Therefore, the AlInGaN-layer investigated here is shown to be homogeneous to this extent.

An attempt was also made to determine the indium and aluminium concentrations by simultaneous evaluation of HAADF intensity and lattice strain measured from the high-resolution STEM images as described by Grieb et al. [32]. However, this method turned out to be less applicable for the AlInGaN material system as is illustrated in Fig. 6: simulations as described above were conducted for various compositions from the two-dimensional concentration space as reference for the intensity. Additionally, the biaxial lattice strain in growth direction was calculated from elasticity theory for comparison with the measured strain. The isolines for both datasets, on which compositions with the same HAADF intensity or the same strain lie, are shown for a fixed specimen thickness of 50 nm. This is a common thickness for quantitative HAADF STEM measurements in the AlGaN/InGaN-system [15]. It becomes apparent that these isolines are nearly parallel, meaning that the information which can be gained from the measurement of HAADF intensity and lattice strain is quasi-equivalent. Even with both quantities measured the simultaneous determination of both the aluminium and the indium concentration is therefore impossible under experimental conditions as two non-equivalent pieces of information would be necessary for this. Using this method the possible compositional range is thus given by a narrow region along the isoline that corresponds to the

measured normalised HAADF intensity.

This concentration range, however, was found to be in full agreement with the other measurements in Table 1 as is illustrated in Fig. 9. For the ternary InGaN layer (composition no. 1), where the prior knowledge of vanishing Al concentration could be utilised to get an exact concentration, the indium concentration was determined to be (11 ± 1) at% and for the AlGaN layer (composition no. 5) (38 ± 1) at% Al was found, which is in excellent agreement with the other methods.

3.3. APT-Analysis

The specimens investigated in the previous section were also examined in a comparative APT study. The measurement conditions were optimised for the material system based on the findings of Mehrtens et al. [33] by cooling down the specimen tip to 20 K and using a laser-pulse energy of 50 pJ at a pulse frequency of 100 kHz for a laser wavelength of 532 nm and a pulse length of $\approx$10 ps. 60 million ions were detected during the entire measurement. Due to the optimisation of acquisition parameters, a III:N-ratio of 52:48 could be achieved, which is close to the expected 1:1 ratio. The deficiency of measured nitrogen has been reported to be due to the dissociation of complex ions between evaporation from the specimen and detection, causing inaccurate identification of incident ions [34,33]. Fig. 7a shows an image of the reconstructed specimen. All five AlInGaN layers were detected entirely. The layer thicknesses and distances are in excellent agreement with the STEM micrographs. An atomic-concentration profile was extracted by averaging in lateral direction and for a bin width of 0.2 nm in growth direction, which is presented in Fig. 7b. The average concentration of each layer is also given in Table 1 and illustrated in Fig. 9, where fair agreement with the EDX results within the according precisions becomes apparent.
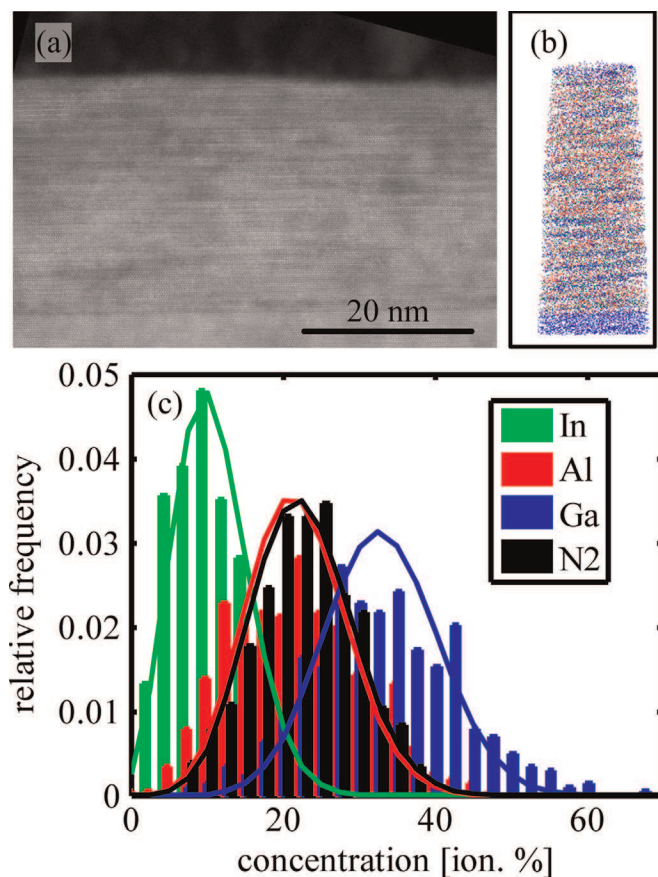
The homogeneity was then statistically investigated similar to the STEM data following Ref. [35]. The volume of each layer was divided into voxels, each containing a fixed number of detected ions. The concentration of each ion species was then calculated and the respective concentration distribution inside each layer was determined. The resulting histograms for Al-, In-, Ga- and N_2-ions for layer no. 4 and voxels containing 40 ions are displayed in Fig. 7c in comparison with the binomial distribution expected for a random alloy. The visibly good fit between both was tested by
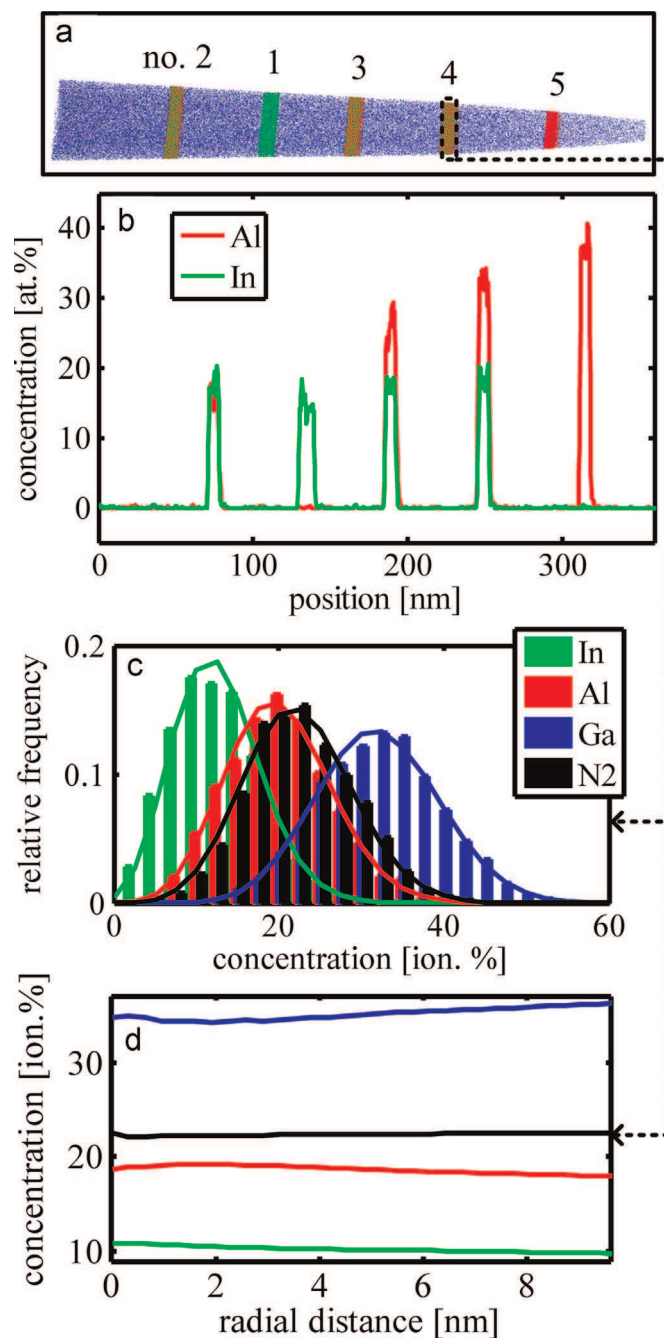
Fig. 7. Evaluation of the APT measurement: the reconstruction of the specimen is shown in (a). (b) displays the resulting concentration profile along the growth direction. In (c) the distribution of various detected ions inside a layer (bars) is compared to the random-alloy expectation (solid curves). (d) is a plot of the ionic concentration in dependence of the radial distance from indium ions. Indications for non-random fluctuations are not found.

Fig. 8. APT evaluation of an inhomogeneous AlInGaN layer: intensity fluctuations between atomic layers were observable in HAADF STEM micrographs as shown in (a), the reconstruction in (b) revealed them to be caused by varying aluminium and gallium concentrations, which caused distinct deviation of measured (bars) and random-alloy (solid curves) distributions in the histogram (c).

the chi-square test and accepted with a significance of 10% for all detected ion types. The test was repeated for voxel sizes of 20, 100 and 200 ions, which corresponds to voxels with approximate side lengths from 1.4 to 3.2 nm. It yielded an identity with a random-alloy distribution with more than 5% significance in all cases. Similar results were obtained for the other layers. Additionally, the radial distribution around indium atoms was investigated by calculating the radially averaged concentration as a function of the distance to a central indium atom and then averaging over all indium atoms. The result is shown in Fig. 7d for layer no. 4: for indium-clustering, one would expect a significant increase in

indium concentration for small radial distances, which was not observed. The radial distribution is almost constant. The APT study hence does confirm the previous findings. All layers are found to be homogeneous on various scales.

To check the power of the previous test, a test structure with a single AlInGaN-layer of a similar composition as no. 4 was investigated with the same parameters as before. Due to a pulsed MOVPE process, which involved an alternating injection of In-, Al- and Ga-precursors, this sample exhibited a stripy appearance in HAADF STEM images caused by monolayers of alternating different compositions, as is shown in Fig. 8a. The stripes are also clearly visible in the APT reconstruction in Fig. 8b, in which they were identified as fluctuations of the aluminium concentration of approximately ± 5 at% with a simultaneously constant indium content. This clearly inhomogeneous sample was also analysed by testing the concentration distributions against the random-alloy expectation with the chi-square test. The corresponding histograms are shown in Fig. 8c. Random distribution of gallium and aluminium was clearly rejected, while it was accepted for indium and nitrogen with a significance of 20%. The test therefore clearly proves its suitability to identify inhomogeneities caused by fluctuations of the magnitude of 10 at% on the sub-nanometer scale.

4. Summary

In conclusion, an investigation of the homogeneity of AlInGaN layers of different concentrations by statistical means using EDX,
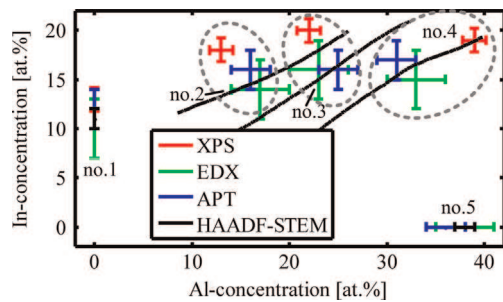
Fig. 9. Overview of the measured concentrations: the results of all investigated compositions from the different methods are marked with their respective errors (see Table 1). The concentration pairs of the quaternary composition nos. 2–4 that are consistent with the measured HAADF STEM intensity are drawn as black iso-lines (only reasonable part was plotted for better readability). The XPS-data was taken from [20]. The values from EDX, HAADF STEM and APT coincide within their error bars.

HAADF STEM and APT was presented. The layers were found to exhibit random-alloy distribution with high significances down to the sub-nanometer scale. The applicability of the tests to the two-dimensional HAADF STEM data was confirmed by additional simulations, in which the statistical power was demonstrated and proved to be comparable to corresponding analyses on three-dimensional APT reconstructions.

The observed increase in width of the PL-emission peak can hence be deducted to stem solely from local concentration fluctuations inherent to a random-alloy distribution of elements. It can be furthermore concluded that, in the studied composition range, the MOVPE parameters used for the growth of the investigated layers do indeed allow epitaxy of homogeneous quaternary AlInGaN without detectable phase separation. With respect to the previous reports of indium cluster formation [10–13] this conclusion does not apply to any growth setup in general. Nevertheless it is shown that homogeneous MOVPE growth of AlInGaN for these concentrations is possible.

Finally, the quaternary concentrations were determined and consistent results were attained as is also illustrated in Fig. 9, where the summarised results of all measurements presented here are seen to coincide within their precisions, though with HAADF STEM, the quaternary composition could not be determined unambiguously, as a second non-equivalent information channel would be needed. Nevertheless, it was demonstrated that the statistical analysis of STEM micrographs by comparison to simulations is sufficiently powerful to exclude the presence of nm-scale chemical species clustering.

References

[1] H. Hirayama, Quaternary InAlGaN-based high-efficiency ultraviolet light-emitting diodes, J. Appl. Phys. 97 (2005) 091101.

[2] M.F. Schubert, J. Xu, J.K. Kim, E.F. Schubert, M.H. Kim, S. Yoon, S.M. Lee, C. Sone, T. Sakong, Y. Park, Polarization-matched GaInNAl–GaInN multi-quantum-well light-emitting diodes with reduced efficiency droop, Appl. Phys. Lett. 93 (2008) 041102.

[3] B. Reuters, A. Wille, N. Ketteniss, H. Hahn, B. Hollnder, M. Heuken, H. Kalisch, A. Vescan, Polarization-engineered enhancement-mode high-electron-

[4] T. Lim, R. Aidam, P. Waltereit, T. Henkel, R. Quay, R. Lozar, T. Maier, L. Kirste, O. Ambacher, GaN-Based submicrometer HEMTs with lattice-matched InAlGaN barrier grown by MBE, IEEE Electron Device Lett. 31 (2010) 671–673.

[5] P.-M. Tu, C.-Y. Chang, S.-C. Huang, C.-H. Chiu, J.-R. Chang, W.-T. Chang, D.-S. Wuu, H.-W. Zan, C.-C. Lin, H.-C. Kuo, C.-P. Hsu, Investigation of efficiency droop for InGaN-based UV light-emitting diodes with InAlGaN barrier, Appl. Phys. Lett. 98 (2011) 211107.

[6] I. Gorczyca, S.P. Łepkowski, T. Suski, N.E. Christensen, A. Svane, Influence of indium clustering on the band structure of semiconducting ternary and quaternary nitride alloys, Phys. Rev. B 80 (2009) 075202.

[7] I. Gorczyca, A. Kamińska, G. Staszczak, R. Czernecki, S.P. Łepkowski, T. Suski, H.P.D. Schenk, M. Glauser, R. Butté, J.-F. Carlin, E. Feltin, N. Grandjean, N. E. Christensen, A. Svane, Anomalous composition dependence of the band gap pressure coefficients in In-containing nitride semiconductors, Phys. Rev. B 81 (2010) 235206.

[8] I. Gorczyca, T. Suski, N.E. Christensen, A. Svane, Band gap bowing in quaternary nitride semiconducting alloys, Appl. Phys. Lett. 98 (2011) 241905.

[9] Z. Chuan-Zhen, Z. Rong, L. Bin, L. Ming, X. Xiang-Qian, X. Zi-Li, Z. You-Dou, A band-gap energy model of the quaternary alloy InGaAlN using modified simplified coherent potential approximation, Chin. Phys. Lett. 30 (2013) 076101.

[10] C.H. Chen, Y.F. Chen, Z.H. Lan, L.C. Chen, K.H. Chen, H.X. Jiang, J.Y. Lin, Mechanism of enhanced luminescence in InAlGaN quaternary epilayers, Appl. Phys. Lett. 84 (2004) 1480–1482.

[11] J. Wu, J. Li, G. Cong, H. Wei, P. Zhang, W. Hu, X. Liu, Q. Zhu, Z. Wang, Q. Jia, L. Guo, Temperature dependence of the formation of nano-scale indium clusters in InAlGaN alloys on Si(111) substrates, Nanotechnology 17 (2006) 1251.

[12] T. Matsuoka, Unstable mixing region in wurtzite InGaAlN, J. Cryst. Growth 189–190 (1998) 19–23.

[13] M. Marques, L.K. Teles, L.M.R. Scolfaro, L.G. Ferreira, J.R. Leite, Microscopic description of the phase separation process in AlGaInN quaternary alloys, Phys. Rev. B 70 (2004) 073202.

[14] J.M. LeBeau, S. Stemmer, Experimental quantification of annular dark-field images in scanning transmission electron microscopy, Ultramicroscopy 108 (2008) 1653–1658.

[15] A. Rosenauer, T. Mehrtens, K. Müller, K. Gries, M. Schowalter, P.V. Satyam, S. Bley, C. Tessarek, D. Hommel, K. Sebald, M. Seyfried, J. Gutowski, A. Avramescu, K. Engl, S. Lutgen, Composition mapping in InGaN by scanning transmission electron microscopy, Ultramicroscopy 111 (2011) 1316–1327.

[16] A. Rosenauer, K. Gries, K. Müller, A. Pretorius, M. Schowalter, A. Avramescu, K. Engl, S. Lutgen, Measurement of specimen thickness and composition in AlGaN/GaN using high-angle annular dark field images, Ultramicroscopy 109 (2009) 1171–1182.

[17] J.P. O'Neill, I.M. Ross, A.G. Cullis, T. Wang, P.J. Parbrook, Electron-beam-induced segregation in InGaN/GaN multiple-quantum wells, Appl. Phys. Lett. 83 (2003) 1965–1967.

[18] A.J. D'Alfonso, B. Freitag, D. Klenov, L.J. Allen, Atomic-resolution chemical mapping using energy-dispersive x-ray spectroscopy, Phys. Rev. B 81 (2010) 100101.

[19] U. Pohl, Methods of epitaxy, in: Epitaxy of Semiconductors, Graduate Texts in Physics, Springer, Berlin, Heidelberg, 2013, pp. 275–313.

[20] J.-P. Ahl, J. Hertkorn, H. Koch, B. Galler, B. Michel, M. Binder, B. Holländer, Morphology, growth mode and indium incorporation of MOVPE grown InGaN and AlInGaN: a comparison, J. Cryst. Growth 398 (2014) 33–39.

[21] L. Giannuzzi, F. Stevie, A review of focused ion beam milling techniques for {TEM} specimen preparation, Micron 30 (1999) 197–204.

[22] T. Mehrtens, S. Bley, P.V. Satyam, A. Rosenauer, Optimization of the preparation of GaN-based specimens with low-energy ion milling for (S)TEM, Micron 43 (2012) 902–909.

[23] K. Thompson, D. Lawrence, D. Larson, J. Olson, T. Kelly, B. Gorman, In situ site-specific specimen preparation for atom probe tomography, Ultramicroscopy 107 (2007) 131–139.

[24] G. Cliff, G.W. Lorimer, The quantitative analysis of thin specimens, J. Microsc. 103 (1975) 203–207.

[25] A. Rosenauer, M. Schowalter, STEMsim A new software tool for simulation of STEM HAADF Z-contrast imaging, in: A.G. Cullis, P.A. Midgley (Eds.), Springer Proceedings in Physics: Microscopy of Semiconducting Materials Conference 2007, Springer, Netherlands, 2007, pp. 170–172.

[26] D.A. Muller, B. Edwards, E.J. Kirkland, J. Silcox, Simulation of thermal diffuse scattering including a detailed phonon dispersion curve, Ultramicroscopy 86 (2001) 371–380 , International Symposium on Spectroscopy of Materials.

[27] A. Rosenauer, M. Schowalter, J.T. Titantah, D. Lamoen, An emission-potential multislice approximation to simulate thermal diffuse scattering in high-resolution transmission electron microscopy, Ultramicroscopy 108 (2008) 1504–1513.

[28] S. Plimpton, Fast parallel algorithms for short-range molecular dynamics, J. Comput. Phys. 117 (1995) 1–19.

[29] M. Schowalter, I. Stoffers, F.F. Krause, T. Mehrtens, K. Müller, M. Fandrich, T. Aschenbrenner, D. Hommel, A. Rosenauer, Influence of static atomic displacements on composition quantification of AlGaN/GaN heterostructures from HAADF-STEM images, Microsc. Microanal. 20 (2014) 1463–1470.

[30] H. Lei, J. Chen, S. Petit, P. Ruterana, X. Jiang, G. Nouet, Stillinger-Weber parameters for In and N atoms, Superlattices Microstruct. 40 (2006) 464–469 (E-

MRS 2006 Symposium S: Material Science and Technology of Wide Bandgap Semiconductors, 2006 Spring Meeting of the European Materials Research Society).

[31] H.W. Lilliefors, On the Kolmogorov–Smirnov test for normality with mean and variance unknown, J. Am. Stat. Assoc. 62 (1967) 399–402.

[32] T. Grieb, K. Müller, E. Cadel, A. Beyer, M. Schowalter, E. Talbot, K. Volz, A. Rosenauer, Simultaneous quantification of indium and nitrogen concentration in InGaNAs using HAADF-STEM, Microsc. Microanal. 20 (2014) 1740–1752.

[33] T. Mehrtens, M. Schowalter, D. Tytko, P. Choi, D. Raabe, L. Hoffmann, H. Jönen, U. Rossow, A. Hangleiter, A. Rosenauer, Measurement of the indium concentration in high indium content InGaN layers by scanning transmission electron microscopy and atom probe tomography, Appl. Phys. Lett. 102 (2013) 132112.

[34] D. Saxey, Correlated ion analysis and the interpretation of atom probe mass spectra, Ultramicroscopy 111 (2011) 473–479 (Special Issue: 52nd International Field Emission Symposium).

[35] M.P. Moody, L.T. Stephenson, A.V. Ceguerra, S.P. Ringer, Quantitative binomial distribution analyses of nanoscale like-solute atom clustering and segregation in atom probe tomography data, Microsc. Res. Tech. 71 (2008) 542–550.